

# Jahn-Teller distortion and magnetic transitions in perovskite $RMnO_3$ ( $R=Ho, Er, Tm, Yb, \text{ and } Lu$ )

Makoto Tachibana,<sup>1</sup> Tomotaka Shimoyama,<sup>2</sup> Hitoshi Kawaji,<sup>2</sup> Tooru Atake,<sup>2</sup> and Eiji Takayama-Muromachi<sup>3</sup><sup>1</sup>ICYS, National Institute for Materials Science, Namiki 1-1, Tsukuba, Ibaraki 305-0044, Japan<sup>2</sup>Materials and Structures Laboratory, Tokyo Institute of Technology, 4259 Nagatsuta-cho, Midori-ku, Yokohama, 226-8503 Japan<sup>3</sup>Advanced Nano Materials Laboratory, National Institute for Materials Science, Namiki 1-1, Tsukuba, Ibaraki 305-0044, Japan

(Received 4 January 2007; revised manuscript received 2 March 2007; published 23 April 2007)

The perovskite  $RMnO_3$  ( $R=Ho, Er, Tm, Yb, \text{ and } Lu$ ) were prepared under high pressure and studied with heat capacity and synchrotron x-ray powder diffraction measurements. The temperature interval between the antiferromagnetic transition and the first-order transition to the presumably  $E$ -type structure narrows with the decreasing ionic radius of  $R$ , and almost closes for  $R=Lu$ . Combined with the data for the larger rare earth  $R$ , the results show intricate relationship between the complex magnetic phase diagram and significant increase of Jahn-Teller distortion found for the smallest members of  $RMnO_3$ .

DOI: 10.1103/PhysRevB.75.144425

PACS number(s): 75.30.Kz, 65.40.Ba, 71.70.Ej, 75.47.Lx

## I. INTRODUCTION

Perovskite manganites  $RMnO_3$  ( $R=\text{rare earth}$ ) are interesting because they show a rich variety of unusual states, arising from the subtle interplay between charge, spin, orbital, and lattice degrees of freedom. Colossal magnetoresistance and charge ordering in hole-doped  $LaMnO_3$  have been the subjects of great interest for the last decade,<sup>1</sup> while recent discoveries of multiferroicity in  $TbMnO_3$  (Ref. 2) and  $DyMnO_3$  (Ref. 3) have created additional excitements in the studies of manganites. These electronic behaviors are all strongly dependent on the underlying lattice, and detailed knowledge on how the properties and structure evolve with  $R$  is expected to provide significant insights into the complex physics of manganites. This study reports on the complete magnetic phase diagram and the evolution of structural parameters for  $RMnO_3$ , and aims to provide basic frameworks for the systematic understanding on this extraordinary system.

Perovskite  $RMnO_3$  is an insulator with the orthorhombic structure (space group  $Pbnm$ ), where the distortion from the ideal cubic structure arises from two sources. One is the mismatch of the  $R$ -O and Mn-O equilibrium bond lengths, and the lattice adjusts to the mismatch by a cooperative rotation (tilting) of the  $MnO_6$  octahedra. This distortion is widely observed in rare-earth perovskites with the  $Pbnm$  structure,<sup>4</sup> where the rotation increases with decreasing ionic radius of  $R$  ( $r_R$ ). For  $RMnO_3$ , the lattice is further distorted by the Jahn-Teller (JT) distortion of the  $MnO_6$  octahedra,<sup>5</sup> which removes the degeneracy of the  $e_g$  orbitals in the  $t_{2g}^3 e_g^1$  electron configuration of  $Mn^{3+}$ . The JT distortion becomes static and long-range ordered below  $T_{JT}$  [ $\sim 750$  K for  $R=La$  (Ref. 6)], where the distribution of long ( $l$ ) and short ( $s$ ) Mn-O bonds in the  $ab$  plane reflects the staggered ordering of  $d_{3x^2-r^2}/d_{3y^2-r^2}$  orbitals,<sup>7</sup> as displayed in the inset of Fig. 1. The orbital ordering pattern is repeated uniformly along the  $c$  axis, with the medium ( $m$ ) Mn-O distance. The JT distortion increases with decreasing  $r_R$  from  $R=La$ ,<sup>8</sup> which is consistent with the increase in  $T_{JT}$  from  $\sim 750$  K for  $R=La$  to  $\sim 1500$  K for  $R=Dy$ .<sup>9</sup> For smaller  $R$ , detailed understanding is lacking since high-pressure or soft-chemistry synthesis is

needed to stabilize these compounds in the perovskite structure.

The continuous evolution of both the octahedral rotation and JT distortion lead one to expect that the magnetic order also evolves smoothly with  $r_R$ . That this is not the case, as shown by Kimura *et al.*<sup>10</sup> for  $R=La-Ho$  and reproduced in Fig. 1, was therefore a great surprise. For  $R=La$ , the in-plane orbital order induces an  $A$ -type antiferromagnetic (AF) order with  $T_N=140$  K, where the spins show ferromagnetic (FM) order in the  $ab$  plane that are stacked antiferromagnetically along the  $c$  axis.  $T_N$  decreases continuously with decreasing  $r_R$  for  $R=La-Gd$ , as expected from the increased distortion. However, for  $R=Eu$  and  $Gd$ , a sinusoidal incommensurate (IC) structure with a temperature-dependent modulation vector  $(0, q, 0)$  precedes the  $A$ -type structure on cooling, and this IC structure continues to emerge with increasing  $q$  ( $0 < q \leq 0.5$ ) for smaller  $R$ .<sup>3,10</sup> Moreover, the  $A$ -type AF structure is no longer the stable ground-state structure for  $R=Tb$  and  $Dy$ ,

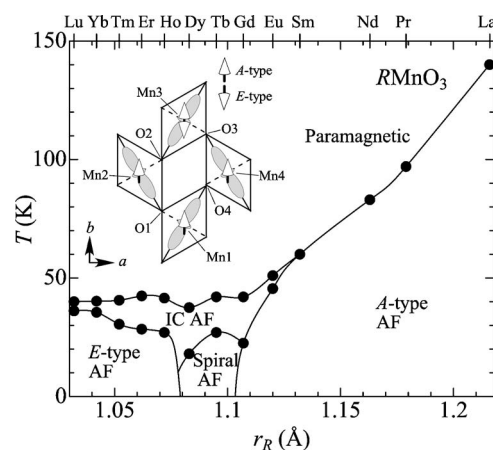


FIG. 1. Magnetic phase diagram for  $RMnO_3$  as a function of the ionic radius of  $R$  ( $r_R$ ). Published data (Ref. 10) are used for  $R=La-Dy$ . Inset shows a sketch of the  $MnO_2$  framework,  $d_{3x^2-r^2}/d_{3y^2-r^2}$  orbitals, and spin-order in the  $ab$  plane. The orbitals are located along the long ( $l$ ) Mn-O bonds, while dashed lines represent the short ( $s$ ) Mn-O bonds. Orbital and spin-order are uniform and staggered, respectively, along the  $c$  axis.

where the IC structure transforms to a transverse spiral structure on cooling.<sup>11,12</sup> The spiral structure breaks the spatial inversion symmetry, leading to ferroelectricity and large magnetoelectric effects in  $R=\text{Tb}$  and  $\text{Dy}$ .<sup>2,3</sup> The spin structure once again changes for  $R=\text{Ho}$ ,<sup>13</sup> where the IC structure locks into an  $E$ -type AF structure with  $q=0.5$ , which is characterized by FM and AF arrangement along the  $a$  and  $b$  axis, respectively. Very recently, ferroelectricity was suggested<sup>14</sup> and shown<sup>15</sup> for  $R=\text{Ho}$ .

The IC phase in  $\text{RMnO}_3$  signals the presence of competing interactions, and Kimura *et al.*<sup>10</sup> invoked the competition between nearest neighbor (NN) FM interaction and next-nearest-neighbor (NNN) AF interaction<sup>13</sup> in the  $ab$  plane to explain the phase diagram. Here, the strength of NN FM interaction is reduced with decreasing  $r_R$ , as the Mn-O-Mn bond angle decreases due to the increased rotation of the  $\text{MnO}_6$  octahedra.<sup>10</sup> Kimura *et al.*<sup>10</sup> emphasized that the increased rotation leads to the reduction of the O2-O4 bond distance (see the inset of Fig. 1), which would particularly strengthen the NNN AF interaction along Mn3-O2-O4-Mn1 (the direction of  $d_{3x^2-y^2}/d_{3y^2-x^2}$  orbitals) over Mn2-O2-O4-Mn4. This results in competition along the  $b$  axis, explaining the IC phase and evolution from the  $A$ -type to  $E$ -type structure with decreasing  $r_R$ . Moreover, the mean-field phase diagram<sup>10</sup> based on these competing interactions showed good agreement with the experiment, supporting the basic idea of the model. On the other hand, Zhou and Goodenough<sup>16</sup> have recently reported the evolution of  $T_N$  and crystal structure for the entire series of  $R$  ( $R=\text{La-Lu}$ ), and concluded that the relevant competition is between FM  $e_g\text{-O-}e_g$  and AF  $t_{2g}\text{-O-}t_{2g}$  interactions in the  $ab$  plane, rather than the AF NNN interaction as proposed by Kimura *et al.* Moreover, they argued<sup>16</sup> that the JT distortion plays the dominant role in determining  $T_N$ , and both the JT distortion and  $T_N$  become insensitive to a change in  $r_R$  for  $R=\text{Ho-Lu}$  with the  $E$ -type structure. While further studies are clearly needed to evaluate these conflicting ideas, we felt that more detailed experiments for  $R=\text{Ho-Lu}$  are in order before additional theories are put forth: The expected IC phase does not appear in Ref. 16, and the large scatter in the reported structural parameters<sup>16,17</sup> can lead to misleading interpretations. With these concerns in mind, we obtain the complete magnetic phase diagram through heat capacity measurements on high-quality samples prepared by the high-pressure technique. Our synchrotron x-ray powder diffraction study reveals the significant increase of JT distortion for the smallest members of  $R$ , providing important perspectives for understanding the complex phase diagram of  $\text{RMnO}_3$ .

## II. EXPERIMENT

Polycrystalline samples of perovskite  $\text{RMnO}_3$  ( $R=\text{Ho, Er, Tm, Yb, and Lu}$ ) were prepared under high pressure. First, pure samples of hexagonal  $\text{RMnO}_3$  were obtained from  $\text{R}_2\text{O}_3$  and  $\text{Mn}_2\text{O}_3$  by solid-state reactions in air. The powders were then sealed in gold capsules and heated to 1573 K for 60 min at 6 GPa in a belt-type press, and rapidly cooled to room temperature before releasing the pressure. There was no significant change in the weight of the capsules, and powder

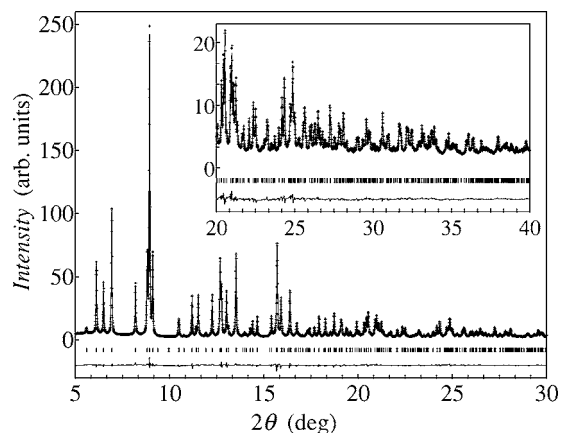


FIG. 2. Observed, calculated, and difference synchrotron x-ray powder diffraction profiles for  $\text{TmMnO}_3$ . Bragg reflections are indicated by tick marks. Inset shows the high angular region in an enlarged scale.

x-ray diffraction showed that the products are of single phase with the orthorhombic perovskite structure. Heat capacity measurements were performed by the relaxation method, using a Quantum Design PPMS. Synchrotron x-ray powder diffraction measurements were performed at 300 K for  $R=\text{Er, Tm, Yb, and Lu}$ , on the BL02B2 beamline at SPring-8 using a wavelength of 0.415 Å. For the measurements, homogeneous powders were obtained by the precipitation method, and these powders were sealed into borosilicate capillaries with an inner diameter of 0.2 mm. Structural parameters were refined by the Rietveld method, using the program RIETAN-2000.<sup>18</sup> No significant deviation from full occupancy was observed, and good reliability factors were obtained in each case. The Rietveld refinement pattern for  $R=\text{Tm}$  is plotted in Fig. 2. The refined structural parameters for  $R=\text{Er-Lu}$  are reported in Table I.

## III. RESULTS AND DISCUSSION

The heat capacity  $C_p$  of  $\text{RMnO}_3$ , measured in both the heating and cooling directions, are shown in Fig. 3. For each compound, a sharp peak at  $T_N \sim 40$  K marks the AF transition into the IC phase. Both the shape of the anomaly and the absence of thermal hysteresis indicate that the AF transition is second order, while the absence of significant rounding testifies to the high quality of the samples. For each  $R$ , additional anomaly is observed at  $T'_N$ , which is 5–15 K below  $T_N$  and ascribed to a lock-in transition to the  $E$ -type structure as reported for  $R=\text{Ho}$ .<sup>13</sup> For this transition, the data taken on the cooling direction show a small anomaly, while the data taken on the heating direction has a larger  $C_p$  and show a sharp peak at  $T'_N$ . The presence of thermal hysteresis indicates that the transition is first order, which is expected for a lock-in transition. Although the anomaly becomes smaller for larger  $R$  and is difficult to be observed for  $R=\text{Ho}$ , a kink at  $T'_N$  is clearly visible when the data are plotted in  $C_p/T$  or  $C_p/T^{1.5}$ , as shown in the inset. It should be noted that  $T_N=41$  K and  $T'_N=27$  K for  $R=\text{Ho}$  are in good agreement with the results obtained on a sample prepared by the soft-

TABLE I. Lattice parameters ( $\text{\AA}$ ), atomic coordinates [ $R$   $4c(x, y, 1/4)$ ; Mn  $4b(0, 1/2, 0)$ ; O<sub>I</sub>  $4c(x, y, 1/4)$ ; O<sub>II</sub>  $8d(x, y, z)$ ], thermal parameters ( $\text{\AA}^2$ ), reliability factors, and selected bond distances ( $\text{\AA}$ ) and bond angles (deg) for  $RMnO_3$  ( $R=\text{Er, Tm, Yb, and Lu}$ ).

$R$	Er	Tm	Yb	Lu
$a$	5.2395(1)	5.2277(1)	5.2163(1)	5.1972(1)
$b$	5.8223(1)	5.8085(1)	5.7991(1)	5.7868(2)
$c$	7.3357(1)	7.3175(2)	7.2992(2)	7.2959(2)
$x(R)$	0.98215(8)	0.98217(9)	0.98217(10)	0.98182(10)
$y(R)$	0.08437(6)	0.08450(7)	0.08481(8)	0.08571(8)
$B(R)$	0.487 (9)	0.590(10)	0.581(11)	0.586(11)
$B(\text{Mn})$	0.37(2)	0.45(2)	0.42(2)	0.38(2)
$x(\text{O}_I)$	0.1138(9)	0.1147(10)	0.1172(11)	0.1206(12)
$y(\text{O}_I)$	0.4607(9)	0.4591(10)	0.4574(11)	0.4583(12)
$B(\text{O}_I)$	0.61(10)	0.70(12)	0.54(13)	0.55(13)
$x(\text{O}_{II})$	0.6997(7)	0.6984(8)	0.6979(9)	0.6989(9)
$y(\text{O}_{II})$	0.3343(7)	0.3372(8)	0.3394(8)	0.3415(8)
$z(\text{O}_{II})$	0.0563(4)	0.0571(5)	0.0580(6)	0.0575(6)
$B(\text{O}_{II})$	0.71(8)	0.83(10)	0.72(10)	0.86(11)
$R_{\text{wp}}$ (%)	3.89	4.00	4.35	4.58
$R_1$ (%)	2.00	2.56	2.73	2.43
$S$	1.72	1.69	1.73	2.37
Mn-O <sub>I</sub> ( $\times 2, m$ )	1.942(2)	1.940(2)	1.940(2)	1.944(2)
Mn-O <sub>II</sub> ( $\times 2, l$ )	2.248(4)	2.255(5)	2.263(5)	2.269(5)
Mn-O <sub>II</sub> ( $\times 2, s$ )	1.891(4)	1.886(4)	1.879(5)	1.862(5)
$\langle \text{Mn-O} \rangle$	2.027	2.027	2.027	2.025
Mn-O <sub>I</sub> -Mn	141.59(2)	141.15(2)	140.27(2)	139.56(2)
Mn-O <sub>II</sub> -Mn ( $\times 2$ )	142.05(5)	141.17(5)	140.51(5)	140.36(5)

chemistry method.<sup>13</sup> For  $R=\text{Lu}$ ,  $C_p$  between 2 and 10 K can be described accurately by  $\beta T^3 + \beta_5 T^5$ , with  $\beta = 0.45 \text{ mJ K}^{-4} \text{ mol}^{-1}$ . This value is larger than  $\beta = 0.19 \text{ mJ K}^{-4} \text{ mol}^{-1}$  for  $R=\text{La}$ ,<sup>19</sup> reflecting the differences in the lattice and/or spin-wave contributions. For  $R=\text{Ho, Er, Tm, and Yb}$ , additional anomaly is observed below 10 K due to the ordering of the  $R^{3+}$  moments.

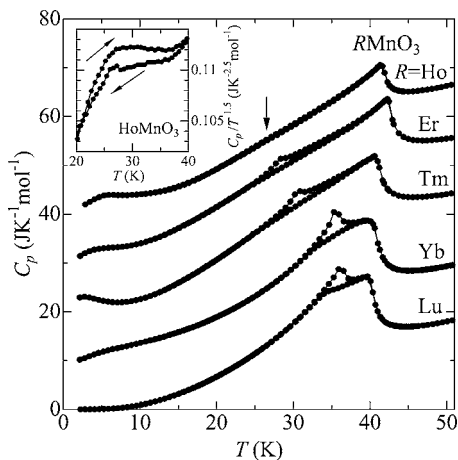


FIG. 3. Heat capacity of  $RMnO_3$  ( $R=\text{Ho, Er, Tm, Yb, and Lu}$ ). The data have been successively offset by  $10 \text{ J K}^{-1} \text{ mol}^{-1}$  for clarity. Inset shows the data in  $C_p/T^{1.5}$  for  $R=\text{Ho}$ .

By combining the present results with the reported data,<sup>10</sup> the magnetic phase diagram for  $RMnO_3$  ( $R=\text{La-Lu}$ ) as a function of  $r_R$  and temperature is obtained as shown in Fig. 1. The phase boundaries show smooth variations with  $r_R$ , with steep boundaries separating the  $A$ -type, spiral, and  $E$ -type AF phases at low temperatures. For  $R=\text{Ho-Lu}$ , the change in  $T_N$  with  $r_R$  is small but smooth, suggesting that the maximum at  $R=\text{Er}$  may be intrinsic. On the other hand,  $T'_N$  shows a gradual increase with decreasing  $r_R$ , almost approaching  $T_N$  for  $R=\text{Lu}$ . Although the magnetic structure for  $R=\text{Er-Lu}$  has not yet been studied in detail,<sup>20</sup> the continuous evolution in  $T'_N$  strongly suggests that the nature of the spin structure does not change in this region. It is noted that the mean-field phase diagram<sup>10</sup> shows similar increase in  $T'_N$  for this region, providing additional support for the basic tenet of the model.

To understand the origin of the magnetic phase diagram, accurate knowledge on the crystal structure is essential. Figure 4 displays the variation of the lattice parameters  $a$ ,  $b$ , and  $c$ , and various Mn-O-Mn bond angles and Mn-O bond distances as a function of  $r_R$ . The present results for  $R=\text{Er-Lu}$  join smoothly with the data<sup>6,8,21</sup> for larger  $R$ , and, unlike the previous study,<sup>16</sup> the data are precise enough to be used in subsequent analysis without imposing any guiding fits. Both the  $a$  and  $c$  axes show continuous decrease with decreasing  $r_R$ , while the  $b$  axis shows a broad maximum at an intermediate  $r_R$ . These behaviors, as well as the relation  $c/\sqrt{2} < a$ ,<sup>4,22</sup>

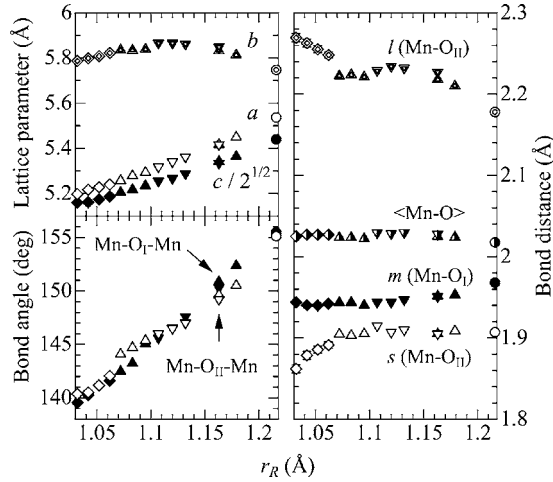


FIG. 4. Variation of the lattice parameters, Mn-O-Mn bond angles, and Mn-O bond distances as a function of  $r_R$ .  $\text{O}_{II}$  is in the  $ab$  plane ( $\text{O}_1\text{-O}_4$  in Fig. 1), while  $\text{O}_I$  is at the apical position along the  $c$  axis. Sources: circle, Ref. 6; triangle, Ref. 8; inverted triangle, Ref. 21; diamond, this study. Data for  $R=\text{Y}$  and  $\text{Er}$  from Ref. 8 are not shown because the samples are nonstoichiometric. The error bars are shown for our results when they are larger than the symbols.

concur with the evolution of the octahedral rotation and JT distortion described below. While the  $\text{Mn-O}_I\text{-Mn}$  bond angle along the  $c$  axis decreases smoothly, the decrease of the  $\text{Mn-O}_{II}\text{-Mn}$  bond angle in the  $ab$  plane becomes weaker when  $b$  reaches the maximum. For  $R=\text{Lu}$ , the latter angle is  $140.4^\circ$ , compared to  $155.1^\circ$  in  $R=\text{La}$ . The Mn-O distances  $l$  and  $s$  in the  $ab$  plane and  $m$  along the  $c$  axis, as well as their average  $\langle \text{Mn-O} \rangle$  also evolve with  $r_R$ . While  $m$  and  $\langle \text{Mn-O} \rangle$  become almost  $r_R$  independent below  $\sim 1.13$  Å, there is significant increase in  $l$  and decrease in  $s$  for  $r_R < 1.07$  Å. The increase in  $l$  is opposite to what was claimed in Ref. 16, though *not* inconsistent with its actual data.<sup>23</sup> As described below, this correction has profound consequences on the understanding of the JT distortion.

The JT distortion for each  $R$  can be evaluated from  $l$ ,  $m$ , and  $s$ , and the results are summarized in Fig. 5.  $Q_2$  and  $Q_3$  are the orthorhombic and tetragonal distortion modes of  $\text{MnO}_6$  octahedra, respectively, and they form orthogonal axes in the  $(Q_2, Q_3)$  plane to describe the potential surface of distortion.<sup>5,16</sup> Here,  $\rho_0$  is a radius in the plane that corresponds to the magnitude of the JT distortion. As the octahedral rotation is superposed on the cooperative JT distortion, the staggered distortion has two minima in the  $(Q_2, Q_3)$  plane with a negative  $Q_3$  and an angle  $\phi$  from the positive and negative  $Q_2$  axes.<sup>5,16</sup>  $Q_2$  increases with decreasing  $r_R$ , with a plateau region at intermediate  $r_R$ . The magnitude of  $Q_3$  also increases with decreasing  $r_R$ , but levels off below  $r_R \sim 1.12$  Å. Consequently,  $\rho_0$  evolves in a manner similar to  $Q_2$ , with a plateau in the same region.  $\phi$  shows a maximum as reported in Ref. 16, but the present results show that the decrease in  $\phi$  below  $r_R \sim 1.10$  Å is due to the increase in  $Q_2$ , rather than a decrease in  $|Q_3|$ .<sup>16</sup> The maximum in  $\phi$ , as well as the plateaus in  $Q_2$  and  $\rho_0$  and the curvature of  $\text{Mn-O}_{II}\text{-Mn}$  bond angle all correspond closely to the broad maximum in

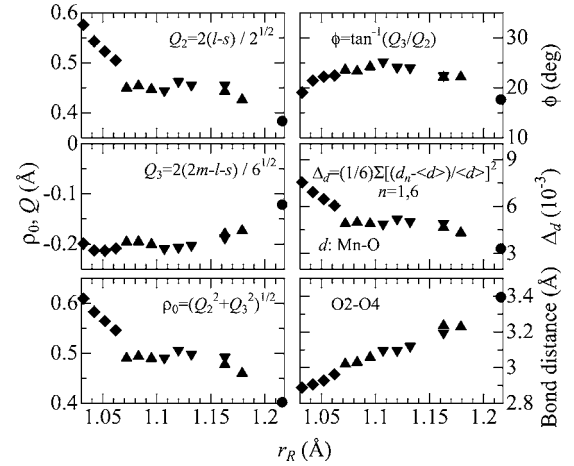


FIG. 5. Evolution of the various parameters associated with JT distortion, and the O2-O4 distance, as a function of  $r_R$ . Symbols are the same as in Fig. 3.

$b$ , which in turn originates from the intrinsic geometric property of the orthorhombic perovskites.<sup>4</sup> As a result of this crystallographic feature, the reduction in  $r_R$  initially increases both the  $Q_2$  and  $Q_3$  distortion modes, but then the distortion is saturated when  $r_R \sim 1.13\text{--}1.08$  Å. Further decrease in  $r_R$  reaches the region where  $b$  decreases significantly, and this is where the strong elongation of the  $\text{MnO}_6$  octahedra in the  $ab$  plane and significant increase in the  $Q_2$  mode take place. (The effect of increasing  $l$  on  $b$  is overcompensated by decreasing  $s$  in the presence of octahedral rotation. See, e.g., Ref. 22.) As previous theories<sup>24</sup> have shown that the JT distortion is stabilized by the octahedral rotation, more detailed calculations incorporating the real structure may fully explain the evolution of JT distortion. The magnitude of the JT distortion is also reflected in  $\Delta_d$ , which measures the deviation of the Mn-O bond length  $d$  from the mean value.  $\Delta_d$  increases with decreasing  $r_R$ , so the previously proposed maximum<sup>25</sup> at  $r_R \sim 1.08$  Å is apparently an artifact caused by the nonstoichiometric samples.<sup>8</sup>

The revised structural parameters have significant implications for the model proposed in Ref. 16. First, the increase in JT distortion for the smallest members of  $R$  implies that the energy splitting of the  $e_g$  orbitals continues to increase with decreasing  $r_R$ , so  $R=\text{Lu}$  should have the largest charge gap<sup>16</sup> with the weakest FM exchange interaction. If the competition between FM  $e_g\text{-O-}e_g$  and AF  $t_{2g}\text{-O-}t_{2g}$  interactions is operative, as suggested in Ref. 16, it may explain the increase in  $T'_N$  for  $R=\text{Ho-Lu}$  but the insensitivity of  $T'_N$  to a change in  $r_R$  remains unclear. Moreover, it is not immediately obvious how the competition involving a single exchange path leads to the observed IC structure. On the other hand, competition with the NNN interaction<sup>10</sup> would naturally explain the phase diagram, since it predicts the IC structure to evolve into the highly distorted members of  $\text{RMnO}_3$ . That  $T'_N$  does not decrease with decreasing  $r_R$  implies that the NNN AF interaction becomes increasingly important. Indeed, the model<sup>10</sup> predicts that the strength of NNN interaction along the  $b$  axis increases faster than the decrease in NN FM interaction for the Mn-O-Mn bond angles from  $\sim 145^\circ$  to  $\sim 130^\circ$ , which would explain the small change in  $T'_N$  for

small  $r_R$ . The increasing importance of the NNN interaction is also corroborated by the O2-O4 distance, which is shown in Fig. 5. Due to the increased rotation of the  $\text{MnO}_6$  octahedra, O2-O4 decreases continuously from 3.40 Å for  $R=\text{La}$  to 2.89 Å for  $R=\text{Lu}$ . As recent first-principles calculations successfully reproduced the  $E$ -type order for  $R=\text{Ho}$ ,<sup>26</sup> further works should establish the bond-length and distortion dependence of the NNN interactions.<sup>27</sup>

#### IV. CONCLUSION

In conclusion, the complete magnetic phase diagram for the perovskite  $\text{RMnO}_3$  ( $R$ =rare earth) has been elucidated by heat capacity measurements on  $R=\text{Ho-Lu}$ . In contrast to the

previous report,<sup>16</sup> the present study reveals the significant increase of JT distortion for the smallest members of  $R$ , and provides additional support for the increasing importance of NNN interactions. Further theories incorporating both the NNN interaction and JT distortion are expected to provide better understanding of the phase diagram.

#### ACKNOWLEDGMENTS

The authors thank A. A. Belik and Y. Kuroiwa for valuable discussions. This study was supported by Special Coordination Funds for Promoting Science and Technology from MEXT, Japan. The experiment at SPring-8 has been carried out with the approval of JASRI.

- 
- <sup>1</sup> *Colossal Magnetoresistive Oxides*, edited by Y. Tokura (Gordon and Breach, London, 2000).
- <sup>2</sup> T. Kimura, T. Goto, H. Shintani, K. Ishizaka, T. Arima, and Y. Tokura, *Nature (London)* **426**, 55 (2003).
- <sup>3</sup> T. Goto, T. Kimura, G. Lawes, A. P. Ramirez, and Y. Tokura, *Phys. Rev. Lett.* **92**, 257201 (2004).
- <sup>4</sup> J.-S. Zhou and J. B. Goodenough, *Phys. Rev. Lett.* **94**, 065501 (2005).
- <sup>5</sup> J. Kanamori, *J. Appl. Phys.* **31**, S14 (1960).
- <sup>6</sup> J. Rodríguez-Carvajal, M. Hennion, F. Moussa, A. H. Moudden, L. Pinsard, and A. Revcolevschi, *Phys. Rev. B* **57**, R3189 (1998).
- <sup>7</sup> Y. Murakami, J. P. Hill, D. Gibbs, M. Blume, I. Koyama, M. Tanaka, H. Kawata, T. Arima, Y. Tokura, K. Hirota, and Y. Endoh, *Phys. Rev. Lett.* **81**, 582 (1998).
- <sup>8</sup> J. A. Alonso, M. J. Martínez-Lope, M. T. Casais, and M. T. Fernández-Díaz, *Inorg. Chem.* **39**, 917 (2000).
- <sup>9</sup> N. V. Kasper and I. O. Troyanchuk, *J. Phys. Chem. Solids* **57**, 1601 (1996).
- <sup>10</sup> T. Kimura, S. Ishihara, H. Shintani, T. Arima, K. T. Takahashi, K. Ishizaka, and Y. Tokura, *Phys. Rev. B* **68**, 060403(R) (2003).
- <sup>11</sup> M. Kenzelmann, A. B. Harris, S. Jonas, C. Broholm, J. Schefer, S. B. Kim, C. L. Zhang, S.-W. Cheong, O. P. Vajk, and J. W. Lynn, *Phys. Rev. Lett.* **95**, 087206 (2005).
- <sup>12</sup> T. Arima, A. Tokunaga, T. Goto, H. Kimura, Y. Noda, and Y. Tokura, *Phys. Rev. Lett.* **96**, 097202 (2006).
- <sup>13</sup> A. Muñoz, M. T. Casáis, J. A. Alonso, M. J. Martínez-Lope, J. L. Martínez, M. T. Fernández-Díaz, *Inorg. Chem.* **40**, 1020 (2001).
- <sup>14</sup> I. A. Sergienko, C. Sen, and E. Dagotto, *Phys. Rev. Lett.* **97**, 227204 (2006).
- <sup>15</sup> B. Lorenz, Y. Q. Wang, and C. W. Chu, cond-mat/0608195 (to be published).
- <sup>16</sup> J.-S. Zhou and J. B. Goodenough, *Phys. Rev. Lett.* **96**, 247202 (2006).
- <sup>17</sup> J.-S. Zhou, J. B. Goodenough, J. M. Gallardo-Amores, E. Morán, M. A. Alario-Franco, and R. Caudillo, *Phys. Rev. B* **74**, 014422 (2006).
- <sup>18</sup> F. Izumi and T. Ikeda, *Mater. Sci. Forum* **321-324**, 198 (2000).
- <sup>19</sup> M. N. Khlopkin, G. Kh. Panova, A. A. Shikov, V. F. Shinyavskii, and D. A. Shulyatev, *Phys. Solid State* **42**, 114 (2000).
- <sup>20</sup> A preliminary study on  $R=\text{Yb}$  [Y. H. Huang, H. Fjellvåg, M. Karppinen, B. C. Hauback, H. Yamauchi, and J. B. Goodenough, *Chem. Mater.* **18**, 2130 (2006)] suggested the  $A$ -type structure, though this was not cited in their subsequent study (Ref. 16).
- <sup>21</sup> T. Mori, N. Kamegashira, K. Aoki, T. Shishido, and T. Fukuda, *Mater. Lett.* **54**, 238 (2002).
- <sup>22</sup> M. W. Lufaso and P. M. Woodward, *Acta Crystallogr., Sect. B: Struct. Sci.* **60**, 10 (2004).
- <sup>23</sup> Reference 16 assumed constant  $m$  and decreasing  $l$  and  $s$  for  $r_R < 1.10$  Å, which is not consistent with its data for  $\langle \text{Mn-O} \rangle$  that increases slightly with decreasing  $r_R$ .
- <sup>24</sup> T. Mizokawa, D. I. Khomskii, and G. A. Sawatzky, *Phys. Rev. B* **60**, 7309 (1999).
- <sup>25</sup> J.-S. Zhou and J. B. Goodenough, *Phys. Rev. B* **69**, 153105 (2004).
- <sup>26</sup> S. Picozzi, K. Yamauchi, G. Bihlmayer, and S. Blügel, *Phys. Rev. B* **74**, 094402 (2006).
- <sup>27</sup> R. Kajimoto, H. Mochizuki, H. Yoshizawa, H. Shintani, T. Kimura, and Y. Tokura, *J. Phys. Soc. Jpn.* **74**, 2430 (2005).